One- and two-*K*-shell vacancy production in atomic Li by 95-MeV/u Ar^{18+} projectiles

J. A. Tanis,[1,2] J.-Y. Chesnel,[1,3] F. Frémont,[3] D. Hennecart,[3] X. Husson,[3] D. Lecler,[3] A. Cassimi,[3] J. P. Grandin,[3] J. Rangama,[3] B. Skogvall,[4] B. Sulik,[5] J.-H. Bremer,[1] and N. Stolterfoht[1]

[1]*Hahn-Meitner-Institut Berlin GmbH, Bereich Strukturforschung, D-14109 Berlin, Germany*

[2]*Department of Physics, Western Michigan University, Kalamazoo, Michigan 49008*

[3]*Centre Interdisciplinaire de Recherche Ions Lasers, Unité Mixte CEA-CNRS-ISMRA et Université de Caen, F-14050 Caen Cedex, France*

[4]*Technische Universität Berlin, Hardenbergstraße 36, D-10623 Berlin, Germany*

[5]*Institute of Nuclear Research (ATOMKI), H-4001 Debrecen, Hungary*

(Received 3 April 2000; published 17 August 2000)

Singly and doubly *K*-shell-vacant states in atomic Li, produced by 95-MeV/u Ar^{18+} projectiles, have been investigated. At this high velocity, excitation and ionization are expected to be well described by perturbation theories. High-resolution spectra for Auger electron emission, occurring in the energy range ~50–90 eV and resulting from the deexcitation of singly or doubly excited states, were measured for various electron emission angles. Both single-*K*-shell excitation and double-*K*-shell vacancy production show strong dependences on the electron emission angle. Experimental anisotropy parameters for the ^2P states resulting from single-*K*-shell excitation are in good agreement with predictions of the Born approximation. In the case of double-*K*-shell-vacancy (i.e., hollow atom) production, the two *K* vacancies are found to come about mainly by ionization plus excitation of the atomic Li target giving rise to excited states in Li^+. Strong line intensities from the $2s^2\ ^1S$ and $2s3s\ ^3S$ excited-state configurations are explained in terms of *shake* processes, providing direct spectral identification for the electron-electron (*e-e*) interaction in producing the doubly vacant *K*-shell configurations. Production of the $2s3s\ ^3S$ state, which has an intensity greater than that of the $2s^2\ ^1S$ state, is attributed to a three-electron transition involving two shake transitions. Production of the $2s2p\ ^3P$ state has a large contribution from the *dielectronic* manifestation of the *e-e* interaction resulting from slow electron emission.

PACS number(s): 34.50.Fa, 32.80.Hd, 32.80.Dz

I. INTRODUCTION

For transitions occurring in fast ion-atom collisions, where the projectile velocity is much greater than the velocity of the active bound electron, the collision interaction is weak so that perturbative methods (e.g., the Born approximation) can be used to treat the collision dynamics. Furthermore, the collision interaction is expected to resemble that of a photon interacting with an atom because the momentum transferred is small [1,2]. Such connections between photoionization and the single ionization of atomic He [3] and atomic Li [4] have recently been investigated experimentally.

For ions traveling near relativistic speeds ($v \sim 100$ a.u.), the interaction time with a target atom is about 10^{-18} s, while single ionization times ($\sim 10^{-16}$ s) and atomic relaxation and autoionization times ($> 10^{-15}$ s) are typically much longer than this. So, the projectile is already far removed from the collision region when the residual target atom (or ion) ''relaxes'' [5], and the ion plays no further role in the subsequent relaxation processes. This separation of the excitation (or ionization) phase of an interaction from the subsequent deexcitation is important because it plays a key role in the interpretation of high-velocity collision phenomena.

Because of their similarity to photon-induced interactions, excitation and ionization by high-velocity projectiles are expected to occur almost exclusively by dipole ($\Delta L = 1$) transitions [1]. Moreover, electron emission which results from *P* to *S* transitions is expected to show the $\sin^2\theta$ (where θ is the electron emission angle relative to the beam direction) angular dependence characteristic of dipole transitions. Thus, high-resolution measurements of Auger-electron emission provide a sensitive probe of the expected connections to photon-induced processes. Such comparisons, as well as deviations from photon-induced expectations, provide important insight into the dynamics of Coulombic interactions between atomic systems at high velocities.

In addition to single transitions, excitation and ionization can be part of multielectron transitions. In ion-atom collisions, multielectron transitions can result from the nucleus-electron (*n-e*) interaction, from the electron-electron (*e-e*) interaction, or from a combination of the two. If a multielectron transition leads to an empty *K* shell, then a so-called ''hollow atom'' (or ion) is produced. Such double-*K*-shell vacancy production in a target atom by fully stripped ion impact can be caused by separate *n-e* interactions, or by an *n-e* interaction followed by an *e-e* interaction. In the former case, the process is referred to as TS2 (two-step with two projectile interactions), and in the latter case it is called TS1 (two-step with one projectile interaction). Because it is mediated by separate *n-e* interactions, TS2 does not require time ordering [6] for the production of two *K* vacancies. On the other hand, for TS1 to take place, a definite time-ordering is required where the *n-e* interaction produces an intermediate state which is the initial state for the subsequent *e-e* process. Moreover, the TS1 process implies dynamic electron correlation [7,8], an effect that is well known in photoionization [9,10], where multielectron transitions resulting from the interaction with a single photon can only be caused by the

e-e interaction. Thus, hollow-atom production by photons corresponds to TS1 in the case of ion impact.

Multielectron transitions in atoms are of importance because they delve into the fundamental nature of atomic structure and dynamics. Specifically, such studies provide information that goes beyond single-electron transition models by probing dynamical electron correlation effects. In recent years, the importance of the electron-electron (*e-e*) interaction in understanding the multiple excitation or ionization of atoms has been widely recognized [7–13]. Furthermore, during the past decade, double-*K*-shell ionization of He by fast ions and photons has attracted much interest [14] due to the insight it provides into dynamic correlation effects.

Early attempts to produce hollow Li with incident ions of intermediate energy were made by Ziem *et al.* [15] and Rødbro *et al.* [16]. More recently, hollow Li has been investigated using photoionization [17–20] and fast ions [21]. In addition to these works, Müller *et al.* [22] have investigated hollow Li production in collisions of Li^+ ions with electrons. Concerning the present work involving fast collisions between highly charged ions and Li atoms, preliminary reports of some aspects of this work have already been published [23–25].

Here, we investigate single-*K*-shell excitation and double-*K*-shell-vacancy production in Li induced by collisions with 95 MeV/u Ar^{18+}. This projectile energy corresponds to $v/c = 0.42$ (v is the ion velocity and c is the speed of light), and a perturbation strength of $Z/v = 0.31$ (in atomic units). This latter value is well within the region of validity of the Born approximation. An important reason for investigating excitation in Li is the fact that both single-and double-*K*-shell vacancy production can be measured in the same experiment via Auger-electron emission (this is not possible for He).

The measurements for single-*K*-shell excitation permit the determination of anisotropy parameters corresponding to Auger emission from the excitation of specific intermediate states. The results are compared with predictions of the Born approximation, which is found to give good agreement as expected at this velocity. For the production of double-*K*-shell vacancies, we find that the resulting ''hollow'' states correspond to configurations in Li^+. Thus, these two-electron configurations come about by *K*-shell ionization plus *K*-shell excitation events. Relatively strong intensities for two-*K*-shell vacancy *S* states are attributed almost wholly to the *e-e* interaction. The *P* states, though found to contain a contribution from the *n-e* interaction, are dominated by the *e-e* interaction as well. Thus, these double-*K*-shell vacancy results provide direct spectral identification of *e-e* interactions in fast ion-atom collisions.

II. EXPERIMENTAL PROCEDURE

The measurements discussed in this work were carried out at the GANIL facility in Caen, France. A schematic of the apparatus is shown in Fig. 1. An intense beam (1–2 μA) of 95 MeV/u Ar^{18+} ions made possible high-resolution measurements for single- and double-*K*-shell vacancy production. The beam was incident on a Li vapor target obtained by heating metallic Li in a small temperature-controlled oven.

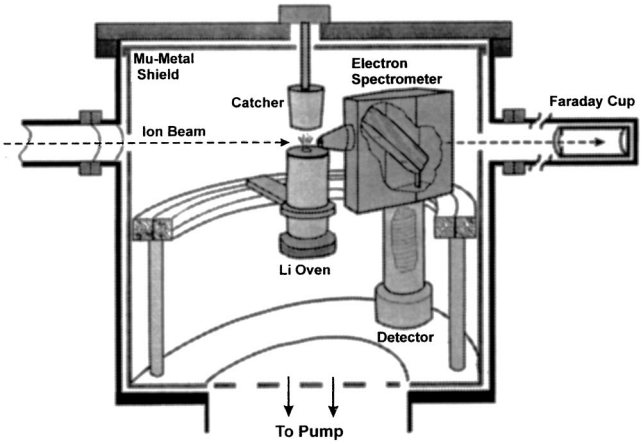

FIG. 1. Schematic of the experimental apparatus.

Li vapor emerging from the oven formed a jet of about 3–4 mm diameter. Continuum electrons emitted from the Li were measured with a parallel-plate electron spectrometer. The scattering chamber and the electron spectrometer were similar to those used previously [4], and more details can be found in Ref. [26].

In connection with the lithium vapor target, several instrumental difficulties had to be solved. First, the metallic lithium had to be heated slowly to drive contaminants from the surface. Then, the lithium temperature was set just high enough above the melting point (180 °C) to obtain a stable jet of Li atoms without producing significant amounts of molecular lithium, i.e., Li_2. In this way, data could be recorded for several hours before it was necessary to refill the oven with lithium. The target thickness for the measurements was estimated to be about 1×10^{14} atoms/cm^2. For the reliable detection of low-energy electrons ($<$100 eV), the possibility of perturbing effects due to the electric and magnetic fields associated with the relatively large current used to heat the metallic lithium, as well as effects due to lithium build-up on the spectrometer surfaces, must be considered. In the former case, measurements were taken with the heating current on and off, and no significant differences were noted in the observed spectra, showing that the measured spectra were not altered by stray fields. In the latter case, an efficient baffle system was used to protect the sensitive parts of the spectrometer. With the procedures used, electron yields could be measured reliably for emission energies as low as 5 eV.

Doubly differential electron yields were measured for *K*-shell Auger-electron emission, which occurs in the range $\sim$50–90 eV, as a function of the emitted electron angle. The spectrometer angle could be varied in the range 25°–160° to determine the angular dependence of the emitted electron yields. To perform the high-resolution Auger measurements, the electrons were decelerated prior to entering the parallel-plate spectrometer.

III. RESULTS AND ANALYSIS

As stated above, electron emission spectra were recorded for 95 MeV/u Ar^{18+} ions colliding with atomic Li. Typical

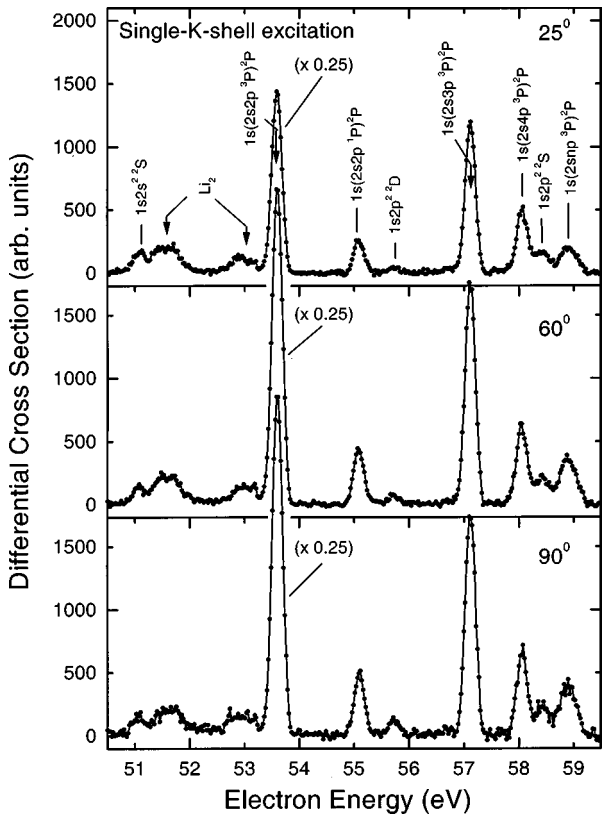

FIG. 2. High-resolution single-*K*-shell excitation Li Auger spectra for electron emission angles of 25°, 60°, and 90° induced by 95 MeV/u Ar^{18+} projectiles. The specific excited-state configurations are indicated. The strongly dominating $1s(2s2p\ ^3P)\ ^2P$ peak has been divided by a factor of 4 for presentation purposes. Note that the singly *K*-shell excited $1s2p^2\ ^2D$ configuration is a doubly excited state ($1s\rightarrow 2p+2s\rightarrow 2p$).

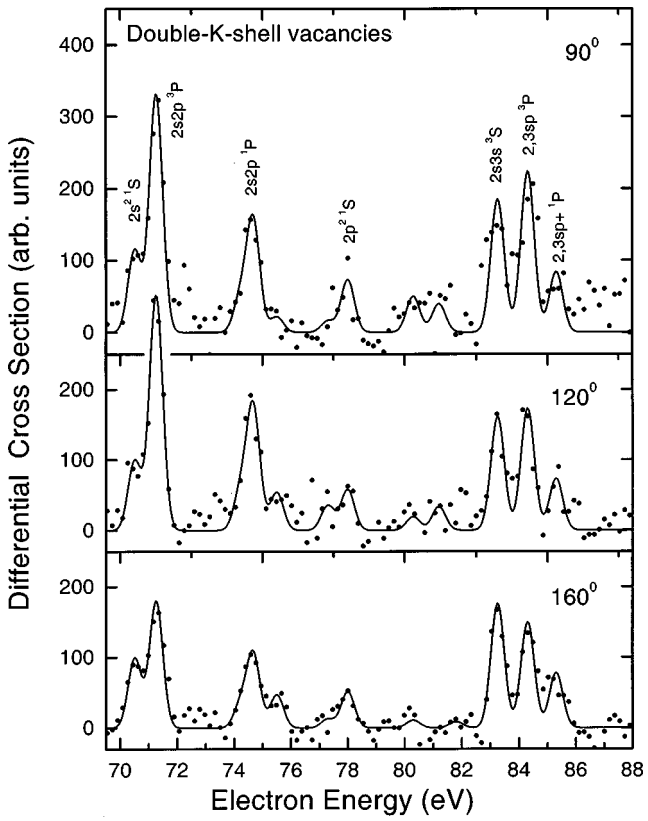

FIG. 3. High-resolution double-*K*-shell vacancy Li Auger spectra for electron emission angles of 90°, 120°, and 160° induced by 95 MeV/u Ar^{18+} projectiles. The observed Auger lines correspond mainly to double-*K*-shell vacancy configurations in excited Li^+ resulting from *K*-shell ionization plus *K*-shell excitation events. The large intensities observed for $2s^2\ ^1S$ and $2s3s\ ^3S$ are particularly significant, as is the fact that the ^3S intensity is greater than the ^1S intensity (see text).

high-resolution spectra for various angles are shown in Fig. 2 for single-*K*-shell excitation and in Fig. 3 for double-*K*-shell vacancy configurations. The energy resolutions for these spectra are 0.25 and 0.55 eV, respectively. Specific states corresponding to the observed Auger-emission lines are indicated. The single-*K*-shell excitation Auger-electron emission lines occur in the range ~50–60 eV, and the double-*K*-shell vacancy lines occur in the range ~70–85 eV. The measured emission spectra were verified to be symmetric with respect to 90°, and this result is taken into account in the angular dependence analysis described below.

The single-*K*-shell excitation spectra of Fig. 2 are seen to be dominated by the strong $1s(2s2p\ ^3P)^2P$ line formed by the $1s\rightarrow 2p$ dipole transition. The corresponding $1s\rightarrow 2s$ monopole transition, giving rise to $1s2s^2\ ^2S$, is found to be about 50 times smaller than the dipole transition. In Fig. 3, the observed double-*K*-shell vacancy Auger lines result primarily from configurations in excited Li^+, indicating that these lines are produced by *K*-shell ionization plus *K*-shell excitation.

Concerning the double-*K*-shell vacancy spectra (Fig. 3), a line due to the $2,3sp\ ^1P$ state (not indicated in the figure) is expected to occur just 0.3 eV higher in energy, at 83.6 eV [16], than the $2s3s\ ^3S$ line at 83.3 eV. With our experimental resolution we should observe intensity from this $2,3sp\ ^1P$ line if it is significant. In the recent work of Diehl *et al.* [27], it is reported that the intensity of the $2,3sp\ ^1P$ line is about 25% that of the $2s3s\ ^3S$ intensity. Close examination of the spectra in Fig. 3 indicates some evidence for emitted electron yield between the $2s3s\ ^3S$ and the $2,3sp\ ^3P$ lines. However, we infer that any contribution due to the $2,3sp\ ^1P$ state does not significantly affect the extracted intensity of the $2s3s\ ^3S$ line. Thus, we conclude that the observed intensity near 83.3 eV is due almost entirely to the $2s3s\ ^3S$ configuration, as indicated in the figure.

For the spectra displayed in Figs. 2 and 3, the background due to continuous electron emission (from direct ionization of the lithium target) has been subtracted. Typically, this background was of the same order of magnitude as the observed peak intensities in the double-*K*-shell vacancy region (Fig. 3). A study of this continuum emission has been published separately [4]. A contribution to the measured Auger intensity from molecular lithium is also observed near 52 eV in Fig. 2. Analysis of the measured spectra shows that this contribution does not exceed 10% of the observed electron yield, however.

Absolute cross sections for the individual lines of Figs. 2

TABLE I. Absolute cross sections for specific single-*K*-shell vacancy states in Li resulting from bombardment by 95 MeV/μ Ar^{18+} projectiles. The listed states correspond to those shown in the spectra of Fig. 2 with the $1s2s2p$ configuration whose main components are $1s(2s2p\ ^3P)^2P$ and $1s(2s2p\ ^1P)^2P$, respectively. Note that the $1s2p^2\ ^2D$ single-*K*-shell vacancy configuration is a doubly excited state ($1s\rightarrow 2p+2s\rightarrow 2p$). The relative uncertainties in the cross sections are less than about $\pm 10\%$. The theoretical values are from the Born approximation [28]. Total cross sections for each configuration were obtained by integrating over the angle assuming a $\sin^2\theta$ dependence for the *P* states and an isotropic dependence for the *S* states (see text).

	Singly differential cross sections (10^{-20} cm^2/sr) Angle				Integrated cross sections (10^{-20} cm^2)		Alignment parameters	
State	25°	60°	90°	120°	Expt.	Theor.[a]	Expt. A_2/A_4	Theor.[b] A_2/A_4
$1s2s^2\ ^2S$	1.2	0.82	0.99	1.0	13	21		
$1s(2s2p\ ^3P)\ ^2_aP$	49	85	89	81	950			
$1s(2s2p\ ^1P)\ ^2_bP$	2.3	3.9	4.3	3.6	44			
$^2_aP+^2_bP$	51	89	93	84	990	970	−0.22	−0.28
$1s2p^2\ ^2D$	0.36	0.75	1.1	0.80	9.5	18	−0.60/+0.09	−0.67/+0.18
$1s2s3p\ ^2P$	10	15	15	15	170	170	−0.15	−0.28
$1s2s4p\ ^2P$	4.5	5.5	5.5	5.8	67	83	−0.09	−0.28
$1s2p^2\ ^2S$	2.0	2.4	2.3	2.3	28	4.8		
$1s2snp\ ^2P$	2.7	4.9	5.2	5.2	57			
Summed	72	120	120	110	1300	1270		

[a]From Ref. [28].

[b]From Refs. [29] and [28]. See also Eqs. (3) and (4).

and 3 were obtained by normalizing to the measured continuum spectra of Ref. [4]. By using the energies available in the literature [15,16] for the main single- and double-*K*-shell vacancy lines in Li, the high-resolution spectra of Figs. 2 and 3 were fit to give relative intensities for each of the observed lines as explained in Ref. [25]. Then, by referring the peak intensities to the continuous electron background, absolute cross sections could be determined for each of the observed Auger lines in Figs. 2 and 3.

The experimentally determined cross sections for single-*K*-shell-excitation and for double-*K*-shell vacancy production are listed in Tables I and II for each of the observed excited states and for each electron ejection angle measured. Also, the ratios for the total (summed over all configurations) double-*K*-shell vacancy production to single-*K*-shell excitation are listed in Table II. The angular distributions for single- and double-*K*-shell vacancy processes are plotted in Figs. 4 and 5, respectively. From these figures, it is seen that

TABLE II. Absolute cross sections for specific double-*K*-shell vacancy states in Li^+ resulting from bombardment by 95 MeV/u Ar^{18+} projectiles. The listed states correspond to those shown in the spectra of Fig. 3. The relative uncertainties in the cross sections are about $\pm 25\%$. Total cross sections were obtained by integrating over the angle assuming a $\sin^2\theta$ dependence for the *P* states and an isotropic dependence for the *S* states. Ratios of double-*K*-shell vacancy production to single-*K*-shell excitation are also listed for each angle, as well as the average ratio for all angles.

	Singly differential cross sections (10^{-20} cm^2/sr) Angle					Integrated cross sections (10^{-20} cm^2)
State	60°	90°	120°	140°	160°	Expt.
$2s^2\ ^1S$	0.36	0.31	0.24	0.26	0.30	3.6
$2s2p\ ^3P$	0.82	0.79	0.83	0.63	0.46	9.3
$2s2p\ ^1P$	0.30	0.37	0.44	0.43	0.26	4.6
$2p^2\ ^1S$	0.053	0.12	0.14	0.16	0.11	1.5
$2s3s\ ^3S$	0.56	0.43	0.51	0.46	0.45	6.0
$2,3sp\ ^3P$	0.51	0.56	0.38	0.19	0.42	5.4
Summed	2.6	2.6	2.5	2.1	2.0	30
						Avg. ratio
Double-*K* to single-*K* ratio (units of 10^{-2})	2.3	2.0	2.2	2.2	2.7	2.3

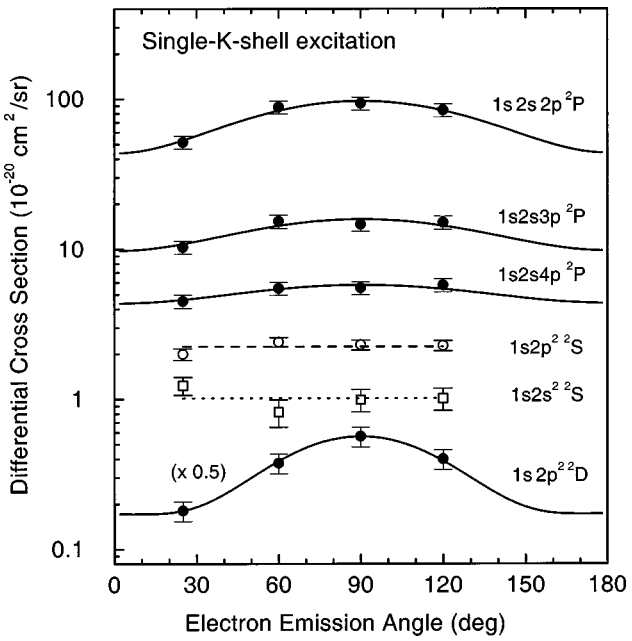

FIG. 4. Single-*K*-shell excitation cross sections, induced by 95 MeV/u Ar^{18+} projectiles, for specific Li excited states vs electron emission angle. The plotted data points are the cross-section values from Table I. The smooth curves are fits to the data using the function $B_0+B_2\sin^2\theta$ for the *P* states. In the case of the doubly excited ^2D state, the function $B_0+B_2\sin^2\theta+B_4\sin^4\theta$ was used (see text). For the *S* states, which are expected to be isotropic, a constant value was fit to the data.

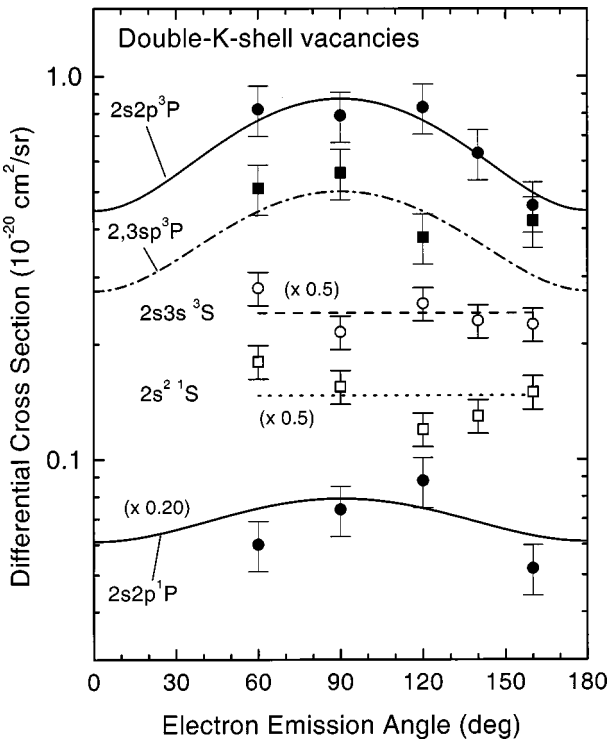

FIG. 5. Double-*K*-shell vacancy cross sections, induced by 95 MeV/u Ar^{18+} projectiles, for specific Li excited states vs electron emission angle. The plotted data points are the cross-section values from Table II. The smooth curves are fits to the data, in the same manner as for Fig. 4, assuming the functional form $B_0+B_2\sin^2\theta$ for the *P* states and a constant value for the *S* states.

the individual state cross sections depend quite strongly on angle, while the double- to single-*K*-shell vacancy ratios, listed in Table II, are essentially independent of angle. This angular dependence of the cross sections is expected, since dipole excitations dominate for the high velocity used here [1]. Total cross sections corresponding to each measured single- and double-*K*-shell vacancy state were obtained by fitting the annular data and then integrating the singly differential cross sections over angle. The fitting results are also shown in Figs. 4 and 5. More will be said about the angular dependence of the cross sections in Sec. IV A below. The resulting total cross sections for each state integrated over angle are listed in Tables I and II, and for single-*K*-shell excitation the cross sections are compared with Born approximation calculations [28]. Comparison of the total single-*K*-shell excitation cross section (1.3×10^{-17} cm^2), summed over all the observed configurations, with the Born theory (1.27×10^{-17} cm^2) gives excellent agreement, as seen from Table I.

IV. DISCUSSION

The predominantly dipole interactions (leading to $L=1$ intermediate states) point to the photon-induced nature of the *K*-shell excitations [1,2]. The good agreement between experiment and the Born theory shows that this approximation can be used with high confidence to extract additional information concerning the excitation of individual magnetic ($M=0,\pm1$) substates, and the resulting anisotropy for Auger-electron emission. For double-*K*-shell vacancy production, electron correlation effects can be identified from the spectral features alone. By calculating the overlap integrals for the initial and final states, i.e., so-called ''shake'' probabilities, the observed relative double-*K*-shell vacancy line intensities can be compared with theoretical expectations. In the following discussion, we treat the cases of single-*K*-shell excitation and double-*K*-shell vacancy production separately.

A. Single-*K*-shell excitation

In an ion-atom collision, the target atom may be excited to an intermediate discrete state that is specified by its orbital angular momentum L and excitation cross section σ_L. This state in turn consists of $2L+1$ degenerate substates associated with the magnetic quantum number M. If the excited state decays via an Auger transition to an *S* state of the residual ion, the angular distribution of the ejected Auger electrons is given by

$$\frac{d\sigma_L}{d\Omega}=\sum_{M=-L}^{L}\sigma_{LM}|Y_{LM}(\Omega)|^2, \tag{1}$$

where $Y_{LM}(\Omega)$ are the spherical harmonics. From symmetry considerations $\sigma_{L,M}=\sigma_{L,-M}$, and since $|Y_{L,M}|^2=|Y_{L,-M}|^2$, Eq. (1) can be written as

$$\frac{d\sigma_L}{d\Omega}=\sigma_{L0}|Y_{L0}(\Omega)|^2+2\sum_{M=1}^{L}\sigma_{LM}|Y_{LM}(\Omega)|^2. \quad (2)$$

This equation, in conjunction with the fits to the data of Figs. 4 and 5, can be used to give values for the excitation cross sections σ_{10} and σ_{11} for the magnetic substates $M=0$ and ±1, respectively. A similar procedure can be used for quadrupole states ($L=2$) to derive values for σ_{20}, σ_{21}, and σ_{22} for the $1s2p^2\ ^2D$ line in Fig. 2.

From the values obtained for σ_{10} and σ_{11}, the anisotropy (or alignment) parameters A_{2n} can be calculated, since the angular distributions $d\sigma_L/d\Omega$ of the emitted electrons can also be written as [29]

$$\frac{d\sigma_L}{d\Omega}\propto\sum_{n=0}^{\infty}A_{2n}P_{2n}(\cos\theta), \quad (3)$$

where the A_{2n} are the anisotropy parameters and the $P_{2n}(\cos\theta)$ are the Legendre polynomials. For instance, for the $L=1$ states shown in Fig. 4, the anisotropy parameter is given by

$$A_2=\frac{\sigma_{10}-\sigma_{11}}{\sigma_{10}+2\sigma_{11}}. \quad (4)$$

From this equation, it is seen that $1\geqslant A_2\geqslant-\frac{1}{2}$. For $A_2=0$, the electron emission is isotropic, while for $A_2=-\frac{1}{2}$, emission occurs only from magnetic states with $M=\pm1$. In the case of the $L=2$ states, corresponding expressions for the anisotropy parameters A_2 and A_4 can be derived [29].

From the fits to the data shown in Fig. 4, we obtain the anisotropy parameters listed in Table I. Also listed are theoretical results obtained from the Born approximation [28]. For the sum of the states corresponding to the $1s2s2p$ configuration, i.e., ${}^2_aP+{}^2_bP$, there is quite reasonable agreement between the experimentally determined value and the calculated value. Furthermore, the relatively large negative value (about half the maximum negative value) found for A_2 shows that the excitation cross section to magnetic substates with $M=\pm1$ is dominant. This largely dominating dipole transition, resulting from the *n-e* interaction, will be important in the discussion of double-*K*-shell vacancy production below.

By comparison, the experimental A_2 values for the $1s2snp\ ^2P$ states ($n=2$, 3, and 4) are seen to decrease significantly with increasing n, indicating that the anisotropy decreases as the principal quantum number increases. This decrease in the anisotropy does not agree with the theory, however, which predicts a constant anisotropy for increasing n. It is likely that this decrease in anisotropy for the higher n states is due to cascade effects where electrons in these higher levels deexcite to lower n levels prior to *K*-Auger emission.

For the $1s2p^2\ ^2D$ quadrupole ($L=2$) state, the relatively large negative value found for A_2 indicates that most of the excitation is to magnetic substates with $M=\pm2$, and this value is in quite good agreement with the theory. The value found for A_4, however, is about half of the theoretical value

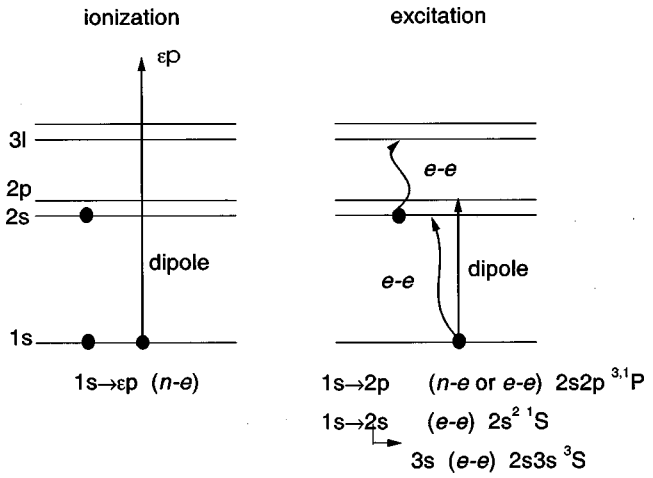

FIG. 6. Schematic showing double-*K*-shell vacancy production in Li. Ionization is assumed to occur first, followed by excitation. The most prominent transitions are shown, as well as the dominant interaction involved (*n-e* or *e-e*) in producing the indicated doubly *K*-shell vacant intermediate excited states.

[29], indicating a smaller excitation to states with $M=0$ than predicted by the theory. Because of the relatively poor counting statistics for this line, and the resulting uncertainties associated with extracting the experimental cross sections ($\sim$40%), we will not consider this discrepancy further here. We note that the $1s2p^2\ ^2D$ state is expected to be produced almost exclusively via sequential *n-e* interactions, and, hence, the intensity of this state provides a measure of the importance of TS2 processes (see the Introduction).

B. Double-*K*-shell vacancy production

1. General considerations

In the case of double-*K*-shell vacancy (hollow Li atom) production, we are primarily interested in the contribution of the *e-e* interaction to the formation of these states. This interaction has two aspects corresponding to whether the first electron is emitted slowly or suddenly. For slow emission, subsequent excitation or ionization of a second electron involves the mutual scattering of two electrons, i.e., it is *dielectronic* in nature, which is a manifestation of dynamic electron correlation [7,8]. On the other hand, sudden emission can result in a subsequent electron transition due to the change in the potential seen by the second active electron as the excited system relaxes [12]. This latter type of transition is a ''mean-field'' effect referred to as a *shake* process.

Double-*K*-shell vacancy production from ground-state Li^0 ($1s\ ^22s$) is shown schematically in Fig. 6. In the figure, ionization via a $1s\rightarrow\varepsilon p$ dipole transition is accompanied by excitation via a $1s\rightarrow2l$ transition (for $l=1$, the excitation is dipole, while for $l=0$ it is monopole), thereby producing two *K*-shell vacancies in Li^+. For fast ions, *n-e* interactions give rise mainly to dipole transitions [1], as seen from the strongly dominant $1s\rightarrow np$ single-*K*-shell excitation lines in Fig. 2. On the other hand, monopole transitions are expected to be induced primarily by the *e-e* interaction since the probability for such transitions via an *n-e* interaction is very small

TABLE III. Calculated shake probabilities for the formation of double-*K*-shell vacancy *S* states in $Li^+(2snl)$, following initial *K*-shell ionization of ground-state neutral Li($1s\,2s$). The overlap integrals for the two-electron initial- and final-state wave functions, obtained from Slater determinants, were calculated within the sudden approximation using the Grant atomic structure code [30]. The initial-state wave functions are taken to be those of ''frozen'' neutral Li, while the wave functions for the final state are taken to be those for relaxed Li^+. In this table, the subscript ''0'' refers to these ''frozen'' neutral Li wave functions. It is noted that two pathways, namely, *direct* and *exchange*, for forming the $2s3s$ configurations are possible (see text).

Transition matrix element	*Direct* probability	*Exchange* probability	Cross term	Total probability
$\lvert\langle 2s^2\ ^1S\rvert 1s_0 2s_0\ ^1S\rangle\rvert^2$	0.0081			0.0081
$3\lvert\langle 2s3s\ ^3S\rvert 1s_0 2s_0\ ^3S\rangle\rvert^2$ [a]	0.00048	0.0090	+0.0042	0.014
$\lvert\langle 2s3s\ ^1S\rvert 1s_0 2s_0\ ^1S\rangle\rvert^2$	0.00016	0.0030	−0.0014	0.0018

[a]The factor of 3 is for the statistical weighting of the triplet state.

[4]. Furthermore, transitions mediated by shake processes (following sudden electron emission) can *only* give rise to $\Delta l=0$ (and $\Delta L=0$) transitions because these processes cause an internal rearrangement of the residual ion, with the consequence that the total orbital angular momentum of the system cannot change.

The double-*K*-shell vacancy spectra presented in Fig. 3 are seen to be dominated by two-electron configurations in Li^+. A spectrum similar to those of Fig. 3 was obtained by Diehl *et al.* [19] for the excitation of Li^0 ($1s^2 2s$) by 197-eV photons, an energy value which lies slightly above the Li^0 double-*K*-shell vacancy threshold. The fact that the spectra of Fig. 3 (and that reported in Ref. [19]) consist mainly of two-electron Li^+ states is significant because it means that double-*K*-shell vacancy events due to *K*-shell ionization plus *K*-shell excitation are much more likely than those due to double-*K*-shell excitation. Furthermore, the total intensity involving $2l3l'$ configurations is seen to be as large as, or even larger than, the total intensity due to $2l2l'$ configurations. This latter observation would not be expected based on independent *n-e* interactions.

2. Shake processes: S states

To explain the large intensities observed for the *S* states, namely, $2s^2\ ^1S$ and $2s3s\ ^3S$, we consider again Fig. 6. The left side shows ionization, due to an *n-e* interaction, occurring via the dipole transition $1s\rightarrow\varepsilon p$ (the monopole transition is negligible). The right side of Fig. 6 shows the subsequent excitation possibilities that are expected to dominate. The most probable excitation mediated by the *n-e* interaction is the dipole transition $1s\rightarrow 2p$, giving rise to the $2s2p\ ^3P$ state (see Fig. 3). Since the probability for a monopole transition ($1s\rightarrow 2s$) via an *n-e* interaction is negligible, the large $2s^2\ ^1S$ double-*K*-shell vacancy intensity can only come from the *e-e* interaction, as is the case for the corresponding photon-induced spectrum reported in the work of Diehl *et al.* [19]. Thus, this line can be used as a benchmark to compare the present data with the photon results and with theoretical calculations. A similar argument applies to the formation of the $2s3s\ ^3S$ configuration, which can only be due to the *e-e* interaction as well. Moreover, we note that ionization must precede excitation for the formation of double-*K*-shell vacancy *S*-state configurations, as initial excitation would give rise to the $1s(2s2p\ ^{3,1}P)^2P$ state (see Fig. 2) which cannot result in the formation of the $2s^2\ ^1S$ or $2s3s\ ^3S$ states via subsequent ionization.

Probabilities for the formation of the $2s^2\ ^1S$ and $2s3s\ ^3S$ states, from the initially ionized $1s2s\ ^{3,1}S$ states, via shake can be calculated within the sudden approximation from the overlap of the two-electron initial- and final-state wave functions, which are obtained from the appropriate Slater determinants. In the sudden approximation, the initial-state wave functions are those of ''frozen'' neutral Li, while the final-state wave functions are those of the relaxed Li^+ ion. These wave functions were obtained using the Grant atomic structure code [30]. The predicted shake results are shown in Table III. In the table we have included results for the $2s3s\ ^1S$ final state, which was not observed in the spectra of Fig. 3. While this latter state cannot be identified in the recorded spectra (this will be discussed below), analysis of it in terms of shake provides additional insight into the interpretation of the observed spectra. We note that, in addition to shake, dielectronic interactions (due to slow electron emission) could contribute to the formation of these states, but such calculations are beyond the scope of the present work.

In the case of $2s^2\ ^1S$, we note that this configuration can only result from the intermediate (''frozen'') $1s_0 2s_0\ ^1S$ configuration, whereby the $1s_0$ electron goes to $2s$ and the $2s_0$ electron remains in the $2s$ orbital of the Li^+ ion. Thus, there is only one pathway for this transition, which we denote as *direct*. Consequently, we use this transition strength as a benchmark for the relative strengths of the other double-*K*-shell vacancy transitions.

For the $2s3s\ ^3S$ and the $2s3s\ ^1S$ states, two possibilities must be considered (see Fig. 6). These configurations can come about by means of a *direct* $1s\rightarrow 3s$ transition (not shown in the figure), or by an *exchange* shake mechanism where the $1s$ electron goes to $2s$ and *simultaneously* the $2s$ electron goes to the $3s$ level, as indicated in the figure.

Considering first the $2s3s\ ^3S$ state, the noteworthy experimental feature is that the intensity of this line is greater than the $2s^2\ ^1S$ intensity (see Fig. 3 and Table II). Since the $2s3s\ ^3S$ configuration is a triplet, it can result only from the intermediate $1s2s\ ^3S$ configuration because this internal re-

TABLE IV. Measured and calculated relative intensities for the various double-*K*-shell vacancy states observed in this work compared with those of Ref. [19]. In each case, the intensities have been normalized to that observed for the $2s^2\ ^1S$ configuration. For the present work, the measured relative intensities were calculated from the experimentally determined angle-integrated cross sections listed in Table II. The calculated relative intensities for the *S* states are from Table III. The relative intensities for the work of Ref. [19] were determined from Fig. 2 of that work.

	Relative intensities		
	Present Work		Ref. [19]
Configuration	Measured	Calculated	Measured
$2s^2\ ^1S$	1	1	1
$2s2p\ ^3P$	2.6		1.1
$2s2p\ ^1P$	1.3		0.80
$2p^2\ ^1S$	0.42		0.18
$2s3s\ ^3S$	1.7	1.7	1.6
$2s3s\ ^1S$		0.22	
$2,3sp\ ^3P$	1.5		1.2

arrangement cannot change the spin angular momentum of the system. For the same reason, this latter state cannot produce the $2s^2$ configuration due to Pauli ''blocking.'' Because there are two pathways, direct and exchange, to the final state for the $2s3s\ ^3S$ and $2s3s\ ^1S$ states, there can be interference between the amplitudes for these processes. The sign and magnitude of this interference are listed as the cross term in Table III.

From the table, it is seen that the exchange mechanism dominates strongly over the direct mechanism for the formation of the $2s3s\ ^3S$ configuration. Thus, we conclude that formation of the $2s3s\ ^3S$ state is principally a *three-step* process involving one *n-e* interaction ($1s \rightarrow \varepsilon p$ ionization) followed by two *e-e* interactions ($1s \rightarrow 2s + 2s \rightarrow 3s$ excitations). Moreover, the interference between the direct and exchange mechanisms gives rise to constructive interference, indicated by the plus sign, further enhancing the strength of this three-step transition. Since a triplet state for the $2s^2$ configuration cannot exist due to the aforementioned Pauli blocking, this constructive interference can be interpreted as the electron from the $1s \rightarrow 2s$ transition ''pushing'' the existing $2s$ electron to $3s$. In other words, the Pauli blocking that prevents the formation of $2s^2\ ^3S$ gives rise to an enhancement, via constructive interference, of the $2s3s\ ^3S$ state to conserve the total transition probability.

The $2s3s\ ^1S$ state, from the calculations shown in Table III, is predicted to be much reduced in overall intensity, by nearly a factor of 8 compared to the triplet state $2s3s\ ^3S$, and by nearly a factor of 5 compared to the $2s^2\ ^1S$ state. There are two reasons for this. First of all, there is the statistical weighting factor that is three times smaller for the singlet state than the triplet state. Second, the cross term for the singlet state gives rise to destructive interference, while the cross term for the triplet state gives rise to constructive interference as discussed above. Thus, the $2s3s\ ^1S$ state, which occurs at ~84.0 eV, is expected to contribute only negligibly to the $2,3sp\ ^3P$ state identified in Fig. 3. This conclusion is corroborated by the photon-induced results reported in Ref. [27].

The measured relative strengths of the *S* states, as well as the *P* states, compared to the $2s^2\ ^1S$ state are listed in Table IV along with the predicted relative cross sections. The predicted strength of $2s3s\ ^3S$ is seen to be in excellent agreement with the measured strength. Values for the photon-induced relative strengths from Ref. [19], for 197 eV, are listed for comparison. It is noted that the values of the relative intensity for the $2s3s\ ^3S$ configuration obtained here and that of Ref. [19] agree very well. The photon energy of 197 eV is significant because it is only slightly above the double-*K*-shell vacancy threshold, and so only slow electrons will be ejected. This is similar to the present case of fast ion-induced electron emission where most of the electrons are emitted with relatively low velocities, corresponding to energies <10 eV. Indeed, the spectrum shown as Fig. 2 of Ref. [19] is quantitatively similar to the spectra shown in Fig. 3 of the present work, with essentially the same excited-state configurations being observed.

3. Dielectronic processes: P states

Finally, we consider the $2s2p\ ^3P$ configuration. While this state can be formed by separate *n-e* interactions ($1s \rightarrow \varepsilon p$ and $1s \rightarrow 2p$), it can also have a contribution from the *e-e* interaction. This latter process takes place if the εp electron, as it leaves the atom, interacts with the remaining $1s$ electron, exciting it to $2p$ while simultaneously giving up its $l=1$ angular momentum to become a continuum $\varepsilon' s$ electron, i.e., $(1s \rightarrow \varepsilon p) \Rightarrow (\varepsilon p + 1s \rightarrow \varepsilon' s + 2p)$, thereby producing the $2s2p\ ^3P$ state via a dielectronic (slow electron) process. We note that this $2s2p\ ^3P$ state cannot be formed via shake since an internal rearrangement cannot change the angular momentum of the residual ion. Dielectronic interactions involving the exchange of angular momentum have been previously observed in low-velocity highly charged ion-atom collisions [31].

Since the $2s2p\ ^3P$ state cannot be produced by shake, identification of the *e-e* contribution to $2s2p\ ^3P$ makes it possible to distinguish experimentally the dielectronic and shake processes. To determine the *e-e* contribution to $2s2p\ ^3P$, we consider again the 197-eV photoinduced electron emission spectrum of Li reported by Diehl *et al.* [19]. In this spectrum, double-*K*-shell vacancy configurations can *only* be produced by the *e-e* interaction (dielectronic or shake) because photons (at least those from a synchrotron source) can interact with only a single electron.

In the present work, the $2s2p\ ^3P$ state can come about through a combination of *n-e* and *e-e* interactions. Since the $2s^2\ ^1S$ line is attributed entirely to the *e-e* interaction (following the initial ionizing *n-e* interaction), the $2s2p\ ^3P$ line induced by fast ions must be at least as large as this same line in the photon-induced spectrum of Ref. [19]. From Table IV, the relative contribution from the $2s2p\ ^3P$ state is seen to be significantly larger in the present work than in the work of Ref. [19]. The excess is attributed to the *n-e* interaction. A similar situation occurs for the $2s2p\ ^1P$ state. These com-

parisons show that the *e-e* interaction plays a significant role in the formation of the double-*K*-shell vacancy ^3P and ^1P states in the present fast ion-atom collision work, and, furthermore, provides spectral identification for the dielectronic (slow electron) process.

Finally, we consider the $2p^2\ ^1S$ configuration at ~78 eV. We note here that in our earlier publication, Ref. [25], we incorrectly identified this line as being due to the double-*K*-shell excitation, three-electron state $2s2p^2\ ^2D$. While this latter state can deexcite by emitting an electron of ~78 eV, the calculations of Chung and Gou [32] indicate that the $2s2p^2\ ^2D$ state deexcites to the $1s2s\ ^3S$, $1s2s\ ^1S$, and $1s2p\ ^3P$ final states with Auger energies of 80.35, 78.45, and 78.09 eV and branching ratios of 48%, 19%, and 33%, respectively. From our measured spectra (Fig. 3), lines at these energies with the predicted relative intensities do not exist, so it is unlikely that the observed line at 78 eV is due to the $2s2p^2\ ^2D$ three-electron configuration. Instead, we attribute this line to the two-electron $2p^2\ ^1S$ configuration in agreement with Ref. [19]. A similar conclusion regarding this 78-eV line was reached by Chung and Gou [32] in their analysis of the Li^+ spectrum reported by Rødbro *et al.* [16].

While the $2p^2\ ^1S$ state can be formed by a combination of ionization plus excitation processes involving *n-e* or *e-e* interactions, a primary consideration for forming this state is the configuration mixing with the $2s^2\ ^1S$ state. A calculation [33] of this mixing based on the Fischer code [34] predicts the $2p^2$ intensity to be 33% of the $2s^2$ intensity, a value which is somewhat larger than that obtained from the data of Ref. [19] as seen in Table IV. On the other hand, in the present work the observed $2p^2$ intensity is about 40% of the $2s^2$ intensity. Consequently, there appears to be a considerable *n-e* contribution to the intensity of the $2p^2\ ^1S$ line at 78 eV in the present fast ion work. We note that this excess intensity cannot be due to *e-e* interactions because then this same excess intensity would appear in the data of Ref. [19].

V. CONCLUSIONS

Single- and double-*K*-shell vacancy configurations in atomic Li, produced by 95 MeV/u Ar^{18+} ions, have been investigated from measurements of the resulting *K*-shell Auger deexcitation spectra. The spectra were recorded in high resolution and measurements were conducted for several electron emission angles, so that anisotropy effects for producing specific excited magnetic substates could be investigated. In the case of double-*K*-shell vacancy production, the emphasis was to determine the role and extent of the electron-electron interaction in producing the two *K*-shell vacancies.

Strong angular dependences of the measured cross sections were observed. For single-*K*-shell excitation of Li by Ar^{18+}, the total excitation cross section and the cross sections for excitation to specific intermediate states are generally in good agreement with predictions of the Born approximation, as expected for the velocities used in this work. For excited *P*-state configurations ($L=1$), the cross sections for magnetic substates with $M=\pm 1$ are found to be dominant and the resulting anisotropy parameters are predicted reasonably well by the theory.

For double-*K*-shell vacancy production in Li by the fast Ar^{18+} projectiles, the two *K* vacancies are found to originate mainly by ionization plus excitation of the Li target. Additionally, the production of $2l3l'$ doubly *K*-shell excited configurations is as large as, or larger than, that for the $2l2l'$ configurations. High-resolution measurements of the double-*K*-shell vacancy Auger lines permit spectral identification of contributions from the electron-electron interaction, and, furthermore, the identification of a correlated three-electron transition.

Double-*K*-shell vacancy configurations attributed to the *e-e* interaction were analyzed in terms of two-electron state ''shake'' calculations, i.e., the overlap integrals for the initial- and final-state configurations. These calculations give results which are generally consistent with the observed intensities of the *S*-state configurations. A significant finding is that the $2s3s\ ^3S$ state comes about mainly by means of a three-electron transition involving an exchange shake process. Analysis of the $2s2p\ ^3P$ intensity indicates that this state is formed largely by the dielectronic *e-e* process following slow electron emission with an additional contribution from *n-e* interactions (shake cannot give rise to this state). Finally, the $2p^2\ ^1S$ line appears to have a significant contribution from *n-e* interactions in addition to that resulting from configuration mixing with the $2s^2\ ^1S$ state.

ACKNOWLEDGMENTS

We acknowledge helpful discussions with Dr. T. W. Gorczyca concerning the configuration mixing of the doubly excited *S* states. We thank Dr. F. Wuilleumier and Dr. D. Cubaynes for helpful discussions concerning the determination of the relative Auger intensities from their photon-induced spectra. This work was supported by the German-French Cooperation Program PROCOPE (Contract No. 98089) and by the German-Hungarian Intergovernmental Collaboration (Project No. B/129). J.-Y.C. was supported by the Alexander von Humboldt Foundation; B.S. was supported by the Hungarian Scientific Research Foundation (OTKA, Grant Nos. T020771 and T016636); J.A.T. was supported by the Division of Chemical Sciences, Office of Basic Energy Sciences, Office of Energy Research, U.S. Department of Energy. We thank the European Commission for financial support during the experiment at the Large European Installation GANIL.

[1] H. A. Bethe, Ann. Phys. (Leipzig) **5**, 325 (1930).

[2] M. Inokuti and Y.-K. Kim, Phys. Rev. **186**, A100 (1969); Y.-K. Kim and M. Inokuti, Phys. Rev. A **1**, 1132 (1970).

[3] R. Moshammer *et al.*, Phys. Rev. Lett. **79**, 3621 (1997).

[4] N. Stolterfoht *et al.*, Phys. Rev. Lett. **80**, 4649 (1998); N. Stolterfoht *et al.*, Phys. Rev. A **59**, 1262 (1999).

[5] This could be likened to the purely classical situation of a fast bullet passing through a strawberry. By the time that the strawberry ''explodes,'' the bullet is already far removed from the interaction region, and, hence, no longer has any influence on the ''relaxing'' strawberry. We acknowledge Professor J. F. Reading for this analogy.
[6] N. Stolterfoht, Phys. Rev. A **48**, 2980 (1993); N. Stolterfoht *et al.*, *ibid.* **48**, 2986 (1993).
[7] N. Stolterfoht, Nucl. Instrum. Methods Phys. Res. B **53**, 477 (1991).
[8] J. F. Reading and A. L. Ford, in *Electronic and Atomic Collisions, Invited Papers*, edited by H. B. Gilbody, W. R. Newell, F. H. Read, and A. C. H. Smith (North-Holland, Amsterdam, 1988), pp. 693–698.
[9] B. Crasemann, J. Phys. (Paris), Colloq. **48**, C9-389 (1987).
[10] B. Crasemann, Comments At. Mol. Phys. **22**, 163 (1989).
[11] See, for example, J. H. McGuire, *Introduction to Dynamic Correlation* (Cambridge University Press, Cambridge, England, 1997).
[12] J. H. McGuire, Phys. Rev. Lett. **49**, 1153 (1982); Phys. Rev. A **36**, 1114 (1987).
[13] F. Martín and A. Salin, Phys. Rev. A **54**, 3990 (1996).
[14] See, for example, J. H. McGuire, N. Berrah, R. J. Bartlett, J. A. R. Samson, J. A. Tanis, C. L. Cocke, and A. S. Schlachter, J. Phys. B **28**, 913 (1995).
[15] P. Ziem, R. Bruch, and N. Stolterfoht, J. Phys. B **8**, L480 (1976).
[16] M. Rødbro, R. Bruch, and P. Bisgaard, J. Phys. B **12**, 2413 (1979).
[17] L. Journel *et al.*, Phys. Rev. Lett. **76**, 30 (1996).
[18] D. Cubaynes *et al.*, Phys. Rev. Lett. **77**, 2194 (1996).
[19] S. Diehl *et al.*, J. Phys. B **30**, L595 (1997).
[20] Y. Azuma *et al.*, Phys. Rev. Lett. **79**, 2419 (1997).
[21] J. A. Tanis, J.-Y. Chesnel, F. Frémont, M. Grether, B. Skogvall, B. Sulik, M. Tschersich, and N. Stolterfoht, Phys. Rev. A **57**, R3154 (1998).
[22] A. Müller *et al.*, Phys. Rev. Lett. **63**, 758 (1989).
[23] N. Stolterfoht, X. Husson, D. Lecler, R. Köhrbrück, B. Skogvall, S. Andriamonje, and J. P. Grandin, in *Abstracts of the Seventeenth International Conference on the Physics of Electronic and Atomic Collisions, Brisbane, Australia, 1991*, edited by W. R. MacGillivray, I. E. McCarthy, and M. C. Standage (AIP, New York, 1991), p. 393.
[24] J. A. Tanis, J.-Y. Chesnel, F. Frémont, D. Hennecart, X. Husson, D. Lecler, A. Cassimi, J. P. Grandin, B. Skogvall, M. Tschersich, B. Sulik, J.-H. Bremer, M. Grether, and N. Stolterfoht, Phys. Scr. **T80**, 381 (1999).
[25] J. A. Tanis, J.-Y. Chesnel, F. Frémont, D. Hennecart, X. Husson, A. Cassimi, J. P. Grandin, B. Skogvall, B. Sulik, J.-H. Bremer, and N. Stolterfoht, Phys. Rev. Lett. **83**, 1131 (1999).
[26] N. Stolterfoht, Z. Phys. **248**, 81 (1971); N. Stolterfoht *et al.*, Europhys. Lett. **4**, 890 (1987).
[27] S. Diehl *et al.*, J. Phys. B **32**, 4193 (1999).
[28] Calculations of excitation were performed using a Born approximation code provided to us by A. Salin (unpublished).
[29] B. Cleff and W. Mehlhorn, J. Phys. B **7**, 593 (1974).
[30] K. G. Dyall, I. P. Grant, C. T. Johnson, F. A. Parpia, and E. P. Plummer, Comput. Phys. Commun. **55**, 425 (1989).
[31] F. W. Meyer, D. C. Griffin, C. C. Havener, M. S. Huq, R. A. Phaneuf, J. K. Swenson, and N. Stolterfoht, Phys. Rev. Lett. **60**, 1821 (1988).
[32] K. T. Chung and B. Gou, Phys. Rev. A **52**, 3669 (1995).
[33] T. Gorczyca (private communication).
[34] C. F. Fischer, Comput. Phys. Commun. **64**, 369 (1991).